Wireless Pers Commun
DOI 10.1007/s11277-011-0493-2

On the Correlation and Ergodic Properties of the Squared Envelope of SOC Rayleigh Fading Channel Simulators

Carlos A. Gutiérrez · Matthias Pätzold

Abstract In this paper, we investigate the correlation and ergodic properties of the squared envelope of a class of autocorrelation-ergodic (AE) sum-of-cisoids (SOC) simulation models for mobile Rayleigh fading channels. Novel closed-form expressions are presented for both the ensemble and the time autocorrelation functions (ACFs) of the SOC simulation model's squared envelope. These expressions have been derived by assuming that the SOC model's inphase and quadrature (IQ) components have arbitrary autocorrelation and cross-correlation properties. This consideration makes the results herein presented more general than those given previously in other papers, where it is assumed that the IQ components of the simulation model are strictly uncorrelated. We show that under certain conditions, the squared envelope of the SOC model is an AE random process. In addition, we evaluate the performance of three fundamental methods for the computation of the model parameters—namely the generalized method of equal areas, the L_p-norm method, and the Riemann sum method—regarding their accuracy for emulating the squared envelope ACF of a reference narrowband Rayleigh fading channel model. The obtained results are important to design efficient simulators for the performance analysis of systems and algorithms sensitive to the correlation properties of the channel's squared envelope, such as speed estimators and handover mechanisms.

Keywords Channel simulators · Ergodic processes · Mobile communications · Rayleigh fading channels · Squared envelope · Sum-of-cisoids · Sum-of-sinusoids

C. A. Gutiérrez
Electronics Department, Autonomous University of San Luis Potosi,
Av. Salvador Nava Mtz. s/n Zona Universitaria, 78290 Mexico, San Luis Potosi, Mexico

C. A. Gutiérrez (✉)
School of Engineering, Universidad Panamericana, Campus Aguascalientes,
Josemaría Escrivá de Balaguer No. 101, 20290 Mexico, Aguascalientes, Mexico
e-mail: cagutierrez@ieee.org

M. Pätzold
Department of Information and Communication Technology, Faculty of Engineering and Science,
University of Agder, P.O. Box 509, 4898 Grimstad, Norway

Published online: 21 January 2012

1 Introduction

Simulation models based on a finite sum of complex sinusoids (cisoids) have widely been used as a basis for the design of efficient mobile fading channel simulators, e.g., see [1–7]. Applications of sum-of-cisoids (SOC) models span from the simulation of narrowband single-input single-output (SISO) channels [1–3], to the development of narrowband [4,5] and wideband [6,7] multiple-input multiple-output (MIMO) fading channel simulators. SOC simulators belong to a special class of simulation models built upon the sum-of-sinusoids (SOS) principle introduced by Rice in [8] and [9]. Roughly speaking, the difference between SOC models and conventional SOS models is that the former models are able to generate complex-valued waveforms with inphase and quadrature (IQ) components having specified autocorrelation and cross-correlation properties [10, Ch. 3]. The latter models, on the other hand, are designed to generate complex-valued waveforms with uncorrelated IQ components [11,12]. Conventional SOS models are therefore limited to the simulation of fading channels characterized by symmetrical Doppler power spectral densities (DPSDs), while SOC models can be applied to the simulation of fading channels having both symmetrical and asymmetrical DPSDs [10]. This is a noteworthy characteristic of the SOC models, as it has been observed from measured data that the DPSD of real-world channels is in general asymmetrical [13,14]. We refer the reader to [10,15] and [16] for further information on the differences between SOC models and SOS models.

Based on the random or deterministic nature of the cisoids' parameters—gains, Doppler frequencies, and phases, we can identify eight fundamental classes of SOC simulation models [15]: Seven classes of stochastic SOC models and one class of deterministic SOC models. Among the seven classes of stochastic SOC models, only the class comprising cisoids with constant gains, constant frequencies, and random phases enables the design of autocorrelation-ergodic (AE) channel simulators. The AE property is highly convenient, as it allows to efficiently approximate the channel's autocorrelation function (ACF) without the need of averaging across simulation runs.

Some important statistical properties of AE SOC simulators for Rayleigh fading channels have been studied in [16] and [17]. The autocorrelation and spectral characteristics of the underlying SOC model as well as the probability density functions (PDFs) of its envelope and phase are analyzed in [16]. The level-crossing rate (LCR) and the average duration of fades (ADF) of the model's envelope are investigated in [17]. Nevertheless, the correlation properties of the squared envelope of AE SOC simulation models have not been studied so far. The squared envelope ACF of the channel gives insights into the instantaneous signal-to-noise ratio (ISNR) fluctuations produced by noisy-fading channels [18, p. 129]. This statistical function exerts a strong influence on the performance of several systems and algorithms for mobile communications, such as speed estimators [19,20] and handover mechanisms [21]. Closing the above mentioned gap is therefore necessary to carry out a reliable laboratory analysis of wireless communication systems sensitive to ISNR fluctuations. It is the aim of this paper to shed some light on the correlation properties of the squared envelope of AE SOC simulators for mobile Rayleigh fading channels.

The contributions of this paper are threefold. Firstly, novel closed-form expressions are presented for the ensemble ACF and the time ACF (TACF) of the SOC simulation model's squared envelope. These expressions have been derived by assuming that the model's IQ components have arbitrary autocorrelation and cross-correlation properties. The obtained expressions are therefore more general than those presented in other papers, where the squared envelope ACF of conventional SOS models is investigated, such as in [11]. Secondly, the ergodic properties of the squared envelope of AE SOC models are studied in this paper for

the first time. Finally, we analyze the performance of three fundamental methods for the computation of the SOC model parameters—namely the generalized method of equal areas (GMEA) [1], the L_p-norm method (LPNM) [6], and the Riemann sum method (RSM) [2]—with respect to their accuracy in emulating the squared envelope ACF of the reference model. Such an analysis had not been made before.

The outline of the paper is as follows. In Sect. 2, we review some relevant statistical properties of a Rayleigh fading channel model that we have adopted as reference model for this research work. In Sect. 3, we analyze the correlation characteristics of the squared envelope of an AE SOC model that is well suited for the simulation of the reference model. In Sect. 4, we evaluate the performance of the parameter computation methods. We present our conclusions in Sect. 5. According to conventions, we will denote stochastic processes and random variables by bold symbols and letters, while constants and deterministic processes will be denoted by plain symbols and letters.

2 The Reference Model

The complex envelope of our reference narrowband Rayleigh fading channel model is mathematically represented in the equivalent baseband by a complex Gaussian random process

$$\boldsymbol{\mu}(t) = \boldsymbol{\mu}_I(t) + j\boldsymbol{\mu}_Q(t), \quad j \triangleq \sqrt{-1} \tag{1}$$

where $\boldsymbol{\mu}_I(t)$ and $\boldsymbol{\mu}_Q(t)$ are stationary zero-mean real-valued Gaussian processes, each with variance $\sigma_{\boldsymbol{\mu}}^2/2$. In line with the 2D scattering model proposed by Clarke [22], we define the random processes in (1) such that their ACFs and cross-correlation functions (CCFs) satisfy the equations [10, Sec. 2.3.1]:

$$r_{\boldsymbol{\mu}_I\boldsymbol{\mu}_I}(\tau) = r_{\boldsymbol{\mu}_Q\boldsymbol{\mu}_Q}(\tau) = \sigma_{\boldsymbol{\mu}}^2 \int_0^{\pi} g_{\boldsymbol{\alpha}}(\alpha) \cos(2\pi f_{\max} \cos(\alpha)\tau) d\alpha \tag{2}$$

$$r_{\boldsymbol{\mu}_I\boldsymbol{\mu}_Q}(\tau) = -r_{\boldsymbol{\mu}_Q\boldsymbol{\mu}_I}(\tau) = \sigma_{\boldsymbol{\mu}}^2 \int_0^{\pi} g_{\boldsymbol{\alpha}}(\alpha) \sin(2\pi f_{\max} \cos(\alpha)\tau) d\alpha \tag{3}$$

$$r_{\boldsymbol{\mu}\boldsymbol{\mu}}(\tau) = 2\,[r_{\boldsymbol{\mu}_I\boldsymbol{\mu}_I}(\tau) + j r_{\boldsymbol{\mu}_I\boldsymbol{\mu}_Q}(\tau)] = 2\sigma_{\boldsymbol{\mu}}^2 \int_0^{\pi} g_{\boldsymbol{\alpha}}(\alpha) \exp(j2\pi f_{\max} \cos(\alpha)\tau) d\alpha \tag{4}$$

where $r_{\boldsymbol{x}\boldsymbol{y}}(\tau) \triangleq E\{\boldsymbol{x}^*(t)\,\boldsymbol{y}(t+\tau)\}$, with $\boldsymbol{x}(t)$ and $\boldsymbol{y}(t)$ denoting two arbitrary random processes. The operators $E\{\cdot\}$ and $(\cdot)^*$ indicate statistical expectation and complex conjugate, respectively. In (2)–(4), $f_{\max}$ designates the maximum Doppler shift and $g_{\boldsymbol{\alpha}}(\alpha) \triangleq [p_{\boldsymbol{\alpha}}(\alpha) + p_{\boldsymbol{\alpha}}(-\alpha)]/2$ is the even part of the PDF $p_{\boldsymbol{\alpha}}(\alpha)$ characterizing the angle-of-arrival (AOA) statistics of the channel. One may observe from (2)–(4) that if the IQ components of $\boldsymbol{\mu}(t)$ are uncorrelated, meaning that $r_{\boldsymbol{\mu}_I\boldsymbol{\mu}_Q}(\tau) = r_{\boldsymbol{\mu}_Q\boldsymbol{\mu}_I}(\tau) = 0$, then the reference model's ACF $r_{\boldsymbol{\mu}\boldsymbol{\mu}}(\tau)$ is a real-valued even function. On the other hand, if $\boldsymbol{\mu}_I(t)$ and $\boldsymbol{\mu}_Q(t)$ are mutually correlated, then $r_{\boldsymbol{\mu}\boldsymbol{\mu}}(\tau)$ is a complex-valued Hermitian symmetric function. Based on the properties of the Fourier transform [23, Sec. 3.6], we can further observe that if $\boldsymbol{\mu}_I(t)$ and $\boldsymbol{\mu}_Q(t)$ are uncorrelated, then the channel's DPSD $S_{\boldsymbol{\mu}\boldsymbol{\mu}}(f) \triangleq \int_{-\infty}^{\infty} r_{\boldsymbol{\mu}\boldsymbol{\mu}}(\tau) \exp\{-j2\pi f\tau\} d\tau$ is real-valued and symmetrical with respect to the origin. Otherwise, if the IQ components of $\boldsymbol{\mu}(t)$ are cross-correlated, then the DPSD $S_{\boldsymbol{\mu}\boldsymbol{\mu}}(f)$ is real-valued and asymmetrical.

Regarding the squared envelope $\boldsymbol{\zeta}^2(t) \triangleq |\boldsymbol{\mu}(t)|^2$ of the reference model, it is shown in [10, Sec. 2.4.3] that $\boldsymbol{\zeta}^2(t)$ is a wide-sense stationary (WSS) process with mean $E\{\boldsymbol{\zeta}^2(t)\} = \sigma_{\boldsymbol{\mu}}^2$ and ACF given as

$$r_{\boldsymbol{\zeta}^2\boldsymbol{\zeta}^2}(\tau) = \sigma_{\boldsymbol{\mu}}^4 + \left|r_{\boldsymbol{\mu}\boldsymbol{\mu}}(\tau)\right|^2. \tag{5}$$

The notation $|\cdot|$ stands for the complex absolute value operator.

3 The SOC Simulation Model

3.1 The Stochastic SOC Simulation Model

The AE SOC simulation model under analysis is characterized by a random process of the form

$$\hat{\boldsymbol{\mu}}(t) = \sum_{n=1}^{N} \hat{c}_n \exp\left\{j(2\pi \hat{f}_n t + \hat{\boldsymbol{\theta}}_n)\right\}. \tag{6}$$

The random phases $\hat{\boldsymbol{\theta}}_n$ are assumed to be mutually independent and uniformly distributed over $[-\pi, \pi)$, the gains $\hat{c}_n$ satisfy $\sum_{n=1}^{N} \hat{c}_n^2 = \sigma_{\boldsymbol{\mu}}^2$, and the Doppler frequencies $\hat{f}_n$ are defined as $\hat{f}_n \triangleq f_{\max}\cos(\hat{\alpha}_n)$, $\hat{\alpha}_n \in [-\pi, \pi)$, $n = 1, 2, \ldots, N$. Numerical results presented in [1,2], and [16] indicate that the correlation properties, the spectral characteristics, and the PDFs of the envelope and phase of the reference model with given correlation properties can efficiently be approximated by means of the SOC model defined in (6). Some important first- and second-order statistics of $\hat{\boldsymbol{\mu}}(t)$ have been analyzed in [16,17]. For the purposes of this paper, it is only relevant to know that if the Doppler frequencies $\hat{f}_n$ satisfy the inequalities

$$\hat{f}_n \neq 0, \quad \forall n \tag{7a}$$

$$\hat{f}_n \neq \hat{f}_m, \quad n \neq m \tag{7b}$$

then $\hat{\boldsymbol{\mu}}(t)$ is a zero-mean WSS process with variance $\sigma_{\boldsymbol{\mu}}^2$ for which the correlation properties can be summarized as [16]:

$$r_{\hat{\boldsymbol{\mu}}_I\hat{\boldsymbol{\mu}}_I}(\tau) = r_{\hat{\boldsymbol{\mu}}_Q\hat{\boldsymbol{\mu}}_Q}(\tau) = \sum_{n=1}^{N} \frac{\hat{c}_n^2}{2}\cos\left(2\pi \hat{f}_n \tau\right) \tag{8}$$

$$r_{\hat{\boldsymbol{\mu}}_I\hat{\boldsymbol{\mu}}_Q}(\tau) = -r_{\hat{\boldsymbol{\mu}}_Q\hat{\boldsymbol{\mu}}_I}(\tau) = \sum_{n=1}^{N} \frac{\hat{c}_n^2}{2}\sin\left(2\pi \hat{f}_n \tau\right) \tag{9}$$

$$r_{\hat{\boldsymbol{\mu}}\hat{\boldsymbol{\mu}}}(\tau) = 2\left[r_{\hat{\boldsymbol{\mu}}_I\hat{\boldsymbol{\mu}}_I}(\tau) + j r_{\hat{\boldsymbol{\mu}}_I\hat{\boldsymbol{\mu}}_Q}(\tau)\right] = \sum_{n=1}^{N} \hat{c}_n^2 \exp\left\{j2\pi \hat{f}_n \tau\right\}. \tag{10}$$

In the previous equations, $\hat{\boldsymbol{\mu}}_I(t) = \Re\{\hat{\boldsymbol{\mu}}(t)\}$ and $\hat{\boldsymbol{\mu}}_Q(t) = \Im\{\hat{\boldsymbol{\mu}}(t)\}$ are the IQ components of $\hat{\boldsymbol{\mu}}(t)$. The operators $\Re\{\cdot\}$ and $\Im\{\cdot\}$ denote the real and the imaginary parts of a complex-valued process, respectively.

For a proper simulation of fading channels characterized by symmetrical DPSDs, the SOC model in (6) has to be parameterized in such a way that its IQ components are mutually uncorrelated, implying that $r_{\hat{\boldsymbol{\mu}}_I\hat{\boldsymbol{\mu}}_Q}(\tau) = r_{\hat{\boldsymbol{\mu}}_Q\hat{\boldsymbol{\mu}}_I}(\tau) = 0$. Assuming the fulfillment of the inequalities in (7), we can deduce from (9) that the random processes $\hat{\boldsymbol{\mu}}_I(t)$ and $\hat{\boldsymbol{\mu}}_Q(t)$ are uncorrelated if and only if (iff):

Condition 1 The number of cisoids N is even, and for each pair of parameters $(\hat{c}_n, \hat{f}_n)$, there exists one and only one pair $(\hat{c}_m, \hat{f}_m)$, such that $\hat{c}_n = \hat{c}_m$ and $\hat{f}_n = -\hat{f}_m$ hold for $n \neq m$ and $n = 1, 2, \ldots, N$.

The previous condition has a strong influence on the TACF of the simulation model's squared envelope, as will be shown in Sect. 3.4. Before we proceed to study this influence, let us analyze first the ensemble ACF of the stochastic SOC simulation model's squared envelope $\hat{\boldsymbol{\xi}}^2(t) \triangleq |\hat{\boldsymbol{\mu}}(t)|^2$.

3.2 The Ensemble ACF of the SOC Model's Squared Envelope

Starting from the definition of the ACF $r_{\hat{\boldsymbol{\xi}}^2\hat{\boldsymbol{\xi}}^2}(\tau)$ of $\hat{\boldsymbol{\xi}}^2(t)$ and using (6), we have

$$\begin{aligned} r_{\hat{\boldsymbol{\xi}}^2\hat{\boldsymbol{\xi}}^2}(\tau) &= E\{|\hat{\boldsymbol{\mu}}(t)|^2 |\hat{\boldsymbol{\mu}}(t+\tau)|^2\} \\ &= \sum_{l=1}^{N}\sum_{m=1}^{N}\sum_{n=1}^{N}\sum_{p=1}^{N} \hat{c}_l\, \hat{c}_m\, \hat{c}_n\, \hat{c}_p \exp\left\{j2\pi(\hat{f}_l - \hat{f}_m)t\right\} \\ &\quad \times \exp\left\{j2\pi(\hat{f}_n - \hat{f}_p)(t+\tau)\right\} E\left\{\exp\left\{j(\hat{\boldsymbol{\theta}}_l - \hat{\boldsymbol{\theta}}_m + \hat{\boldsymbol{\theta}}_n - \hat{\boldsymbol{\theta}}_p)\right\}\right\}. \end{aligned} \tag{11}$$

Since the random phases $\hat{\boldsymbol{\theta}}_n$ are mutually independent and uniformly distributed over $[-\pi, \pi)$, the expectation in (11) is different from zero only if: $l = m = n = p$; $l = m, n = p, l \neq n$; and $l = p, m = n, l \neq m$. Bearing this in mind, we obtain

$$\begin{aligned} r_{\hat{\boldsymbol{\xi}}^2\hat{\boldsymbol{\xi}}^2}(\tau) = & \underbrace{\sum_{l=1}^{N} \hat{c}_l^4}_{\text{Case: } l=m=n=p} + \underbrace{\sum_{m=1}^{N}\sum_{\substack{n=1 \\ n\neq m}}^{N} \hat{c}_m^2 \hat{c}_n^2}_{\text{Case: } l=m,\ n=p,\ l\neq n} \\ & + \underbrace{\sum_{p=1}^{N}\sum_{\substack{q=1 \\ q\neq p}}^{N} \hat{c}_p^2\, \hat{c}_q^2 \exp\left\{-j2\pi \hat{f}_p \tau\right\} \exp\left\{j2\pi \hat{f}_q \tau\right\}}_{\text{Case: } l=p,\ m=n,\ l\neq m}. \end{aligned} \tag{12}$$

The previous result can be rearranged as follows

$$r_{\hat{\boldsymbol{\xi}}^2\hat{\boldsymbol{\xi}}^2}(\tau) = \left[\sum_{m=1}^{N} \hat{c}_m^2\right]^2 - \sum_{n=1}^{N} \hat{c}_n^4 + \sum_{p=1}^{N}\sum_{q=1}^{N} \hat{c}_p^2\, \hat{c}_q^2 \exp\{-j2\pi \hat{f}_p \tau\} \exp\{j2\pi \hat{f}_q \tau\}. \tag{13}$$

Since the cisoids' gains $\hat{c}_n$ satisfy the condition $\sum_{n=1}^{N} \hat{c}_n^2 = \sigma_{\boldsymbol{\mu}}^2$, and given that $r_{\hat{\boldsymbol{\mu}}\hat{\boldsymbol{\mu}}}(\tau) = \sum_{n=1}^{N} \hat{c}_n^2 \cdot \exp\{j2\pi \hat{f}_n \tau\}$ [see (10)], we can finally write

$$r_{\hat{\boldsymbol{\xi}}^2\hat{\boldsymbol{\xi}}^2}(\tau) = \sigma_{\boldsymbol{\mu}}^4 + |r_{\hat{\boldsymbol{\mu}}\hat{\boldsymbol{\mu}}}(\tau)|^2 - \sum_{n=1}^{N} \hat{c}_n^4. \tag{14}$$

One can easily verify that the mean value of $\hat{\boldsymbol{\xi}}^2(t)$ is equal to $E\{\hat{\boldsymbol{\xi}}^2(t)\} = \sigma_{\boldsymbol{\mu}}^2$. Thus, we can conclude that $\hat{\boldsymbol{\xi}}^2(t)$ is a WSS process because its mean value is constant over time and its ACF $r_{\hat{\boldsymbol{\xi}}^2\hat{\boldsymbol{\xi}}^2}(\tau)$ is time-shift insensitive.

By comparing (14) with (5), we can observe that to accurately emulate the squared envelope ACF $r_{\boldsymbol{\zeta}^2\boldsymbol{\zeta}^2}(\tau)$ of the reference model, the SOC model in (6) has to be parameterized in such a way that $r_{\hat{\boldsymbol{\mu}}\hat{\boldsymbol{\mu}}}(\tau) \approx r_{\boldsymbol{\mu}\boldsymbol{\mu}}(\tau)$ and $\sum_{n=1}^{N} \hat{c}_n^4 \approx 0$. Several different parameter computation methods that render a good approximation to $r_{\boldsymbol{\mu}\boldsymbol{\mu}}(\tau)$ have been proposed in the literature, e.g., those described in [1] and [2]. However, none of the existing methods is designed to minimize the factor $\sum_{n=1}^{N} \hat{c}_n^4$. To ensure that this factor is negligible, a large number of cisoids, say $N \geq 50$, has to be considered.

3.3 The Deterministic SOC Simulation Model

In practice, the simulation of the reference model is performed by generating sample functions of $\hat{\boldsymbol{\mu}}(t)$. The output of the simulator can therefore be represented by a deterministic process having the form

$$\hat{\mu}^{(k)}(t) = \sum_{n=1}^{N} \hat{c}_n \exp\left\{ j\left(2\pi \hat{f}_n t + \hat{\theta}_n^{(k)}\right)\right\} \tag{15}$$

where k is a positive integer and $\hat{\theta}_n^{(k)}$ is the outcome of $\hat{\boldsymbol{\theta}}_n$ associated to the kth sample function of $\hat{\boldsymbol{\mu}}(t)$. The time characteristics[1] of $\hat{\mu}^{(k)}(t)$ are investigated in [10, Sec. 3.4.3]. Here, it is only important to know that if the inequalities in (7) hold, then the TACF of $\hat{\mu}^{(k)}(t)$ can be expressed as

$$r_{\hat{\mu}^{(k)}\hat{\mu}^{(k)}}(\tau) = \sum_{n=1}^{N} \hat{c}_n \exp\left\{ j2\pi \hat{f}_n \tau\right\}, \quad \forall k \tag{16}$$

where $r_{xy}(\tau) \triangleq \langle x^*(t) y(t+\tau)\rangle$, with $x(t)$ and $y(t)$ denoting two arbitrary functions of time. Notice that the TACF $r_{\hat{\mu}^{(k)}\hat{\mu}^{(k)}}(\tau)$ of any sample function $\hat{\mu}^{(k)}(t)$ is equal to the ensemble ACF $r_{\hat{\boldsymbol{\mu}}\hat{\boldsymbol{\mu}}}(\tau)$ [cf. (16) and (10)].

3.4 The TACF of the SOC Model's Squared Envelope

With respect to the TACF $r_{\hat{\zeta}^{(k)^2}\hat{\zeta}^{(k)^2}}(\tau)$ of the sample functions $\hat{\zeta}^{(k)^2}(t)$ of $\hat{\boldsymbol{\zeta}}^2(t)$, we have

$$\begin{aligned} r_{\hat{\zeta}^{(k)^2}\hat{\zeta}^{(k)^2}}(\tau) &= \left\langle |\hat{\mu}^{(k)}(t)|^2 |\hat{\mu}^{(k)}(t+\tau)|^2 \right\rangle \\ &= \sum_{l=1}^{N}\sum_{m=1}^{N}\sum_{n=1}^{N}\sum_{p=1}^{N} \hat{c}_l\, \hat{c}_m\, \hat{c}_n\, \hat{c}_p \exp\left\{ j2\pi(\hat{f}_n - \hat{f}_p)\tau\right\} \\ &\quad \times \exp\left\{ j(\hat{\theta}_l - \hat{\theta}_m + \hat{\theta}_n - \hat{\theta}_p)\right\} \\ &\quad \times \lim_{T\to\infty} \frac{1}{2T} \int_{-T}^{T} \exp\left\{ j2\pi(\hat{f}_l - \hat{f}_m + \hat{f}_n - \hat{f}_p)t\right\} dt. \end{aligned} \tag{17}$$

In order to find a compact closed-form expression for $r_{\hat{\zeta}^{(k)^2}\hat{\zeta}^{(k)^2}}(\tau)$, we will assume that in addition to the inequalities in (7), the following condition is met:

[1] The time average of a function $x(t)$ is denoted by $\langle x(t)\rangle$ and defined as $\langle x(t)\rangle \triangleq \lim_{T\to\infty} \frac{1}{2T} \int_{-T}^{T} x(t)dt$.

Condition 2 If $N \geq 4$, then the Doppler frequencies $\hat{f}_n$ are pair-wise different in the sense that:

$$\hat{f}_l + \hat{f}_n = \hat{f}_m + \hat{f}_p, \quad \text{iff} \begin{cases} l = m = n = p; \\ \text{or } l = m, n = p, l \neq n; \\ \text{or } l = p, m = n, l \neq m. \end{cases} \tag{18}$$

Under such conditions, the integral in (17) is different from zero only if: $l = m = n = p$; $l = m, n = p, l \neq n$; and $l = p, m = n, l \neq m$. By solving (17) for these three cases, we find that [cf. (12)]:

$$\begin{aligned} r_{\hat{\zeta}^{(k)2}\hat{\zeta}^{(k)2}}(\tau) &= \sum_{l=1}^{N} \hat{c}_l^4 + \sum_{m=1}^{N} \sum_{\substack{n=1 \\ n\neq m}}^{N} \hat{c}_m^2 \hat{c}_n^2 + \sum_{p=1}^{N} \sum_{\substack{q=1 \\ q\neq p}}^{N} \hat{c}_p^2 \hat{c}_q^2 \exp\left\{-j2\pi \hat{f}_p \tau\right\} \exp\left\{j2\pi \hat{f}_q \tau\right\} \\ &= \sigma_{\boldsymbol{\mu}}^4 + \left|r_{\hat{\mu}^{(k)}\hat{\mu}^{(k)}}(\tau)\right|^2 - \sum_{n=1}^{N} \hat{c}_n^4. \end{aligned} \tag{19}$$

Note that the results presented in (19) and (14) are equal, as $r_{\hat{\mu}^{(k)}\hat{\mu}^{(k)}}(\tau) = r_{\hat{\boldsymbol{\mu}}\hat{\boldsymbol{\mu}}}(\tau) \forall k$.

We pointed out in Sect. 3.1 that the IQ components of $\hat{\boldsymbol{\mu}}(t)$ are mutually uncorrelated iff the Doppler frequencies $\hat{f}_n$ and the gains $\hat{c}_n$ satisfy Condition 1. For such a particular case, the solution given in (19) for $r_{\hat{\zeta}^{(k)2}\hat{\zeta}^{(k)2}}(\tau)$ is not valid, because Condition 1 is not compatible with Condition 2. This is because the equation $\hat{f}_l + \hat{f}_n = \hat{f}_m + \hat{f}_p$ has more solutions than the ones specified in (18) if Condition 1 is fulfilled. Notice that Condition 1 implies that the Doppler frequencies $\hat{f}_n$ are given such that $\hat{f}_n \neq \hat{f}_m \; \forall n \neq m$ and $\hat{f}_n = -\hat{f}_{N-n+1}, n = 1, 2, \ldots, N$, where it has been assumed that $\hat{f}_n < \hat{f}_m$ for $n < m$. Thus, the equality in (18) holds in this case also if $l \neq n \neq m \neq q, m = N - l + 1$, and $q = N - n - 1$.

The simulation of fading channels having uncorrelated IQ components is relevant for many practical purposes, e.g., for analyzing the system performance under isotropic scattering conditions. For this reason, we derive in the Appendix a solution for $r_{\hat{\zeta}^{(k)2}\hat{\zeta}^{(k)2}}(\tau)$ by neglecting Condition 2 and assuming the fulfillment of Condition 1. We suppose without loss of generality that the Doppler frequencies $\hat{f}_n$ are indexed such that $\hat{f}_n < \hat{f}_m \; \forall n < m$. The solution derived in the Appendix has the following structure

$$\begin{aligned} r_{\hat{\zeta}^{(k)2}\hat{\zeta}^{(k)2}}(\tau) = \sigma_{\boldsymbol{\mu}}^4 + \left|r_{\hat{\mu}^{(k)}\hat{\mu}^{(k)}}(\tau)\right|^2 - \sum_{n=1}^{N} \hat{c}_n^4 + 4 \Bigg\{ \Bigg| \sum_{m=1}^{M} \hat{c}_m^2 \cos\left(2\pi \hat{f}_m \tau\right) \\ \times \exp\left\{ j \left(\hat{\theta}_m^{(k)} + \hat{\theta}_{N-m+1}^{(k)} \right) \right\} \Bigg|^2 - \sum_{k=1}^{M} \hat{c}_k^4 \cos^2\left(2\pi \hat{f}_k \tau\right) \Bigg\} \end{aligned} \tag{20}$$

where $M = N/2$ (N is even). It should be noticed that the expression presented above depends on the phases $\hat{\theta}_n^{(k)}$. This is in contrast to the solution given in (19), which is not influenced by the parameters $\hat{\theta}_n^{(k)}$.

3.5 Ergodic Properties of the SOC Model's Squared Envelope

On the basis of the results presented so far, we can analyze the ergodicity of the simulation model's squared envelope $\hat{\boldsymbol{\zeta}}^2(t)$. To start with, we recall that a WSS random process is said to be AE if all TACFs of the sample functions are equal to the ensemble ACF of the underlying

stochastic process [24, Sec. 6.6]. Clearly, the stochastic simulation model described by $\hat{\boldsymbol{\mu}}(t)$ is AE, since $r_{\hat{\mu}^{(k)}\hat{\mu}^{(k)}}(\tau) = r_{\hat{\boldsymbol{\mu}}\hat{\boldsymbol{\mu}}}(\tau) \forall k$ [cf. (10) and (16)].

From the results presented in Sects. 3.2 and 3.4, we can conclude that if Condition 2 is fulfilled, then $\boldsymbol{\zeta}^2(t)$ is an AE process, as $r_{\hat{\zeta}^{(k)^2}\hat{\zeta}^{(k)^2}}(\tau) = r_{\hat{\boldsymbol{\zeta}}^2\hat{\boldsymbol{\zeta}}^2}(\tau) \forall k$. However, if the simulation model is parameterized such that its IQ components are uncorrelated, implying that Condition 1 is satisfied, then the TACF $r_{\hat{\zeta}^{(k)^2}\hat{\zeta}^{(k)^2}}(\tau)$ of the kth sample function of $\hat{\boldsymbol{\zeta}}^2(t)$ is a function of the phases $\hat{\theta}_n^{(k)}$. In this case, $\hat{\boldsymbol{\zeta}}^2(t)$ is not an AE process, since the equality $r_{\hat{\zeta}^{(k)^2}\hat{\zeta}^{(k)^2}}(\tau) = r_{\hat{\boldsymbol{\zeta}}^2\hat{\boldsymbol{\zeta}}^2}(\tau)$ is not valid for all values of k.

4 Performance Evaluation of the Parameter Computation Methods

The accuracy of the SOC simulation model to emulate the statistical properties of the reference model is ultimately determined by the method employed to compute the gains $\hat{c}_n$ and the Doppler frequencies $\hat{f}_n$. The GMEA [1], the LPNM [6], and the RSM [2] have been proposed as suitable parameter computation methods for the design of SOC simulators for fading channels characterized by any given (symmetrical or asymmetrical) DPSD. In this section, we evaluate the performance of these methods in terms of the emulation of the reference model's squared envelope ACF. We also present some numerical results that demonstrate the correctness of the expressions derived in the previous section for $r_{\hat{\boldsymbol{\zeta}}^2\hat{\boldsymbol{\zeta}}^2}(\tau)$ and $r_{\hat{\zeta}^{(k)^2}\hat{\zeta}^{(k)^2}}(\tau)$.

4.1 Review of the Parameter Computation Methods

4.1.1 The GMEA

To allow for a proper emulation of the channel's envelope distribution, the GMEA defines the gains $\hat{c}_n$ as follows [1], [10, Sec. 4.3]

$$\hat{c}_n = \frac{\sigma_{\boldsymbol{\mu}}}{\sqrt{N}}, \quad n = 1, 2, \ldots, N. \tag{21}$$

The Doppler frequencies $\hat{f}_n$ are obtained by finding the roots of the equation

$$\int_{-f_{\max}}^{\hat{f}_n} S_{\boldsymbol{\mu}\boldsymbol{\mu}}(f)\, df - \frac{\sigma_{\boldsymbol{\mu}}^2}{N}\left(N - n + \frac{1}{2}\right) = 0 \tag{22}$$

for $n = 1, 2, \ldots, N$.

4.1.2 The LPNM

For this method, the gains are given as in (21). However, to maximize the quality of the approximation $r_{\boldsymbol{\mu}\boldsymbol{\mu}}(\tau) \approx r_{\hat{\boldsymbol{\mu}}\hat{\boldsymbol{\mu}}}(\tau)$ over a given interval of interest centered at the origin, say $\tau \in [-\tau_{\max}, \tau_{\max}]$, the Doppler frequencies $\hat{f}_n$ are computed as minimizers of the L_p-norm [5,6]

$$\varepsilon_{r_{\boldsymbol{\mu}\boldsymbol{\mu}}}^{(p)} \triangleq \left\{ \frac{1}{\tau_{\max}} \int_0^{\tau_{\max}} \left| r_{\boldsymbol{\mu}\boldsymbol{\mu}}(\tau) - r_{\hat{\boldsymbol{\mu}}\hat{\boldsymbol{\mu}}}(\tau) \right|^p d\tau \right\}^{1/p} \tag{23}$$

where p is a positive integer. For our experiments, we will set $p = 2$ and $\tau_{\max} = N/(4 f_{\max})$.

4.1.3 The RSM

For the RSM, it is assumed that the PDF $p_{\boldsymbol{\alpha}}(\alpha)$ of the AOA α is given such that its even part $g_{\boldsymbol{\alpha}}(\alpha)$ is non-singular and has at most one maximum in $[0, \pi)$. Under this assumption, the gains $\hat{c}_n$ and the AOAs $\hat{\alpha}_n$, which are related to the Doppler frequencies $\hat{f}_n$ via $\hat{f}_n = f_{\max} \cos(\hat{\alpha}_n)$, are defined as follows [2]:

$$\hat{c}_n = \sigma_{\boldsymbol{\mu}} \sqrt{\frac{g_{\boldsymbol{\alpha}}(\hat{\alpha}_n)}{\sum_{m=1}^{N} g_{\boldsymbol{\alpha}}(\hat{\alpha}_m)}} \tag{24}$$

$$\hat{\alpha}_n = \alpha_\ell + \frac{\alpha_u - \alpha_\ell}{N} \left(n - \frac{1}{2} \right), \quad \alpha_u > \alpha_\ell \tag{25}$$

for $n = 1, 2, \ldots, N$. In (25), α_ℓ and α_u designate the lower and the upper boundaries of the subinterval $\mathscr{I}_U$ of $[0, \pi)$ inside of which the function $g_{\boldsymbol{\alpha}}(\alpha)$ is above a given threshold $\gamma_q \in (0, \sup\{g_{\boldsymbol{\alpha}}(\alpha)\})$, where $\sup\{\cdot\}$ denotes the supremum. The value of γ_q is defined as a percentage q of the supremum of $g_{\boldsymbol{\alpha}}(\alpha)$, i.e.,

$$\gamma_q = \sup\{g_{\boldsymbol{\alpha}}(\alpha)\} \times \frac{q}{100}, \quad 0 < q < 100. \tag{26}$$

A good trade-off between the approximations to the channel's ACF and envelope distribution can be obtained by choosing $q \in [0.1, 1]$. In this paper, we will consider $q = 0.5$.

It is worth mentioning that the Doppler frequencies $\hat{f}_n$ obtained by applying any of the aforementioned methods satisfy in general the inequalities in (7) [10, Ch. 4]. The methods are therefore well suited for the design of AE SOC channel simulators. Furthermore, if the DPSD $S_{\boldsymbol{\mu}\boldsymbol{\mu}}(f)$ of the reference model is asymmetrical, then the application of such methods results, in the majority of cases, in a set of Doppler frequencies that meet Condition 2. On the other hand, for the GMEA and the RSM, it is shown in [10, Appx. E] that Condition 1 is always fulfilled if the channel's DPSD $S_{\boldsymbol{\mu}\boldsymbol{\mu}}(f)$ is symmetrical.

4.2 Simulation Set-Up

We evaluate the methods' performance by assuming that the channel's AOA statistics follows the von Mises distribution [25]. The von Mises PDF is given as $p_{\boldsymbol{\alpha}}(\alpha) = \exp\{\kappa \cos(\alpha - m_\alpha)\} / (2\pi I_0(\kappa))$ for $\alpha \in [-\pi, \pi)$, where $m_\alpha \in [-\pi, \pi)$ is the mean AOA, $\kappa \geq 0$ determines the channel's angular spread, and $I_0(\cdot)$ denotes the zeroth-order modified Bessel function of the first kind. When using the von Mises distribution, the ACF of the reference model can be expressed in closed form as [25]

$$r_{\boldsymbol{\mu}\boldsymbol{\mu}}(\tau) = \frac{\sigma_{\boldsymbol{\mu}}^2}{I_0(\kappa)} I_0\Big(\Big\{ \kappa^2 - (2\pi f_{\max}\tau)^2 + j4\pi\kappa f_{\max} \cos(m_\alpha)\tau \Big\}^{1/2} \Big). \tag{27}$$

We carry out our investigations by considering the following values for the pair of parameters (m_α, κ): $(0°, 0)$; $(0°, 5)$; $(0°, 20)$; $(0°, 10)$; $(30°, 10)$; and $(90°, 10)$. The first and the last pair of parameters are representative of fading channels characterized by symmetrical DPSDs, whereas the other four pairs correspond to channels with asymmetrical DPSDs [10, Sec. 2.5.1]. For the simulations, we will consider $f_{\max} = 91\,\text{Hz}$ and $\sigma_{\boldsymbol{\mu}}^2 = 1$.

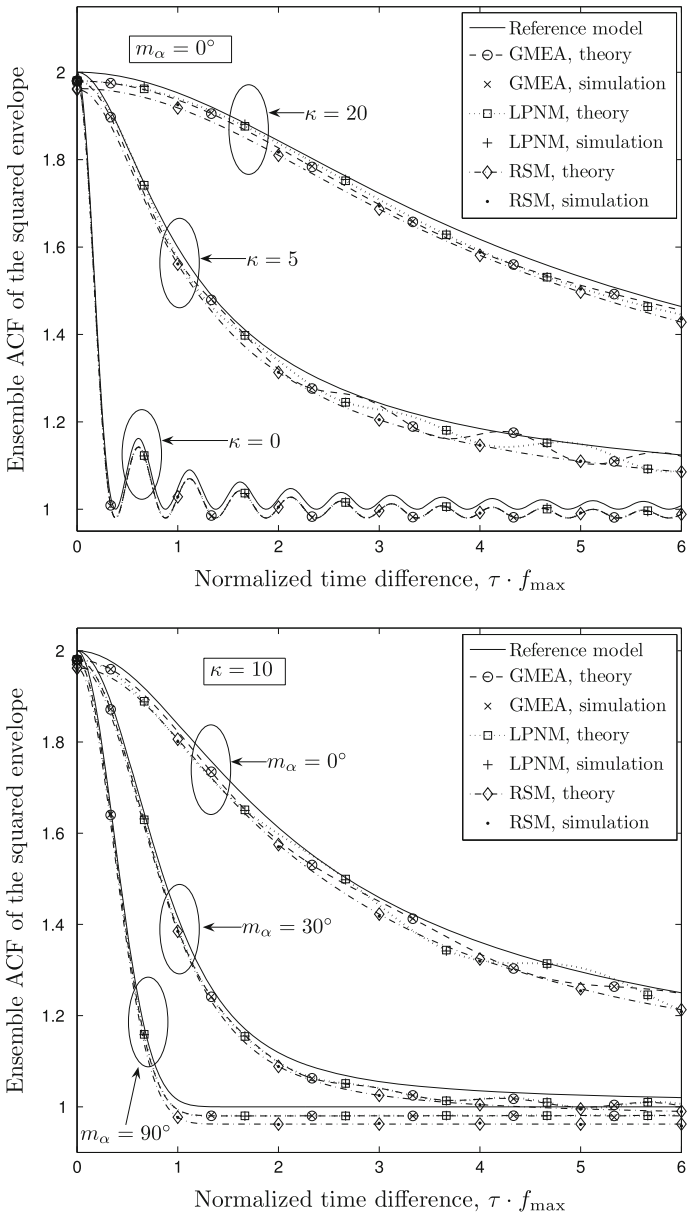

Fig. 1 Comparison among the GMEA, the LPNM, and the RSM in terms of the emulation of the ensemble ACF of the reference model's squared envelope by considering the von Mises PDF of the AOA ($f_{\max} = 91$ Hz, $\sigma^2_{\boldsymbol{\mu}} = 1$, and $N = 50$)

4.3 Simulation Results and Discussion

In Fig. 1, we present a comparison between the squared envelope ACF of the reference model, $r_{\boldsymbol{\zeta}^2\boldsymbol{\zeta}^2}(\tau)$, and the squared envelope ACF of the simulation model, $r_{\hat{\boldsymbol{\zeta}}^2\hat{\boldsymbol{\zeta}}^2}(\tau)$, with $N = 50$. The

figure shows theoretical and empirical graphs of the ensemble ACF of $\hat{\boldsymbol{\zeta}}^2(t)$. The theoretical curves were obtained by evaluating (14), whereas the empirical graphs were generated by averaging over the measured ACFs of 100 simulated sample functions of $\hat{\boldsymbol{\zeta}}^2(t)$. Such an averaging was necessary, since the process $\hat{\boldsymbol{\zeta}}^2(t)$ is not always AE.[2] However, to demonstrate the correctness of the solutions presented in Sect. 3.4 for the TACF $r_{\hat{\zeta}^{(k)2}\hat{\zeta}^{(k)2}}(\tau)$ of the sample functions of $\hat{\boldsymbol{\zeta}}^2(t)$, we present in Fig. 2 a comparison between analytical and empirical graphs of $r_{\hat{\zeta}^{(k)2}\hat{\zeta}^{(k)2}}(\tau)$ generated by applying the RSM. One can observe from Figs. 1 and 2 that the results obtained in practice are in excellent agreement with the ones predicted by the theory. Furthermore, the graphs depicted in Fig. 2 show that the process $\hat{\boldsymbol{\zeta}}^2(t)$ is AE if the DPSD $S_{\boldsymbol{\mu}\boldsymbol{\mu}}(f)$ is asymmetrical, and non-AE if $S_{\boldsymbol{\mu}\boldsymbol{\mu}}(f)$ is symmetrical. This is in line with the observations we made in Sect. 3.5—we recall that the RSM satisfies Condition 2 if $S_{\boldsymbol{\mu}\boldsymbol{\mu}}(f)$ is asymmetrical, and it fulfills Condition 1 if $S_{\boldsymbol{\mu}\boldsymbol{\mu}}(f)$ is symmetrical [see Sect. 4.1].

With respect to the methods' performance, we can see in Fig. 1 that all three methods provide a reasonably good approximation to $r_{\boldsymbol{\zeta}^2\boldsymbol{\zeta}^2}(\tau)$. However, the best fitting to the ACF of $\hat{\boldsymbol{\zeta}}^2(t)$ is achieved by the GMEA and the LPNM. For illustration, we plot in Fig. 3 the root-mean square (RMS) error

$$\varepsilon^{(2)}_{r_{\boldsymbol{\zeta}^2\boldsymbol{\zeta}^2}} \triangleq \left\{ \frac{1}{\tau_{\max}} \int_0^{\tau_{\max}} \left| r_{\boldsymbol{\zeta}^2\boldsymbol{\zeta}^2}(\tau) - r_{\hat{\boldsymbol{\zeta}}^2\hat{\boldsymbol{\zeta}}^2}(\tau) \right|^2 d\tau \right\}^{1/2} \tag{28}$$

between $r_{\boldsymbol{\zeta}^2\boldsymbol{\zeta}^2}(\tau)$ and $r_{\hat{\boldsymbol{\zeta}}^2\hat{\boldsymbol{\zeta}}^2}(\tau)$ by considering $\tau_{\max} = N/(4f_{\max})$. Figure 3 shows clearly that the GMEA and the LPNM produce a smaller error than the RSM. Furthermore, the graphs of $\varepsilon^{(2)}_{r_{\boldsymbol{\zeta}^2\boldsymbol{\zeta}^2}}$ depicted in Fig. 3 indicate that the GMEA and the LPNM perform essentially the same.

A quick inspection of the curves drawn in Fig. 1 reveals that regardless of the underlying parameter computation method, there exists an offset between the ACFs of $\hat{\boldsymbol{\zeta}}^2(t)$ and $\boldsymbol{\zeta}^2(t)$. Such an offset, which can clearly be distinguished at $\tau = 0$, is caused by the negative term $-\sum_{n=1}^{N} \hat{c}_n^4$ affecting the ACF $r_{\hat{\boldsymbol{\zeta}}^2\hat{\boldsymbol{\zeta}}^2}(\tau)$ of $\hat{\boldsymbol{\zeta}}^2(t)$ [see (14)]. One may observe from Fig. 1 that the smallest offset is produced by the GMEA and the LPNM, and the largest by the RSM. This can be seen in Fig. 4, where we have plotted the absolute value of the negative factor $-\sum_{n=1}^{N} \hat{c}_n^4$ as a function of N. A comparison between the graphs depicted in Figs. 1 and 3 reveals that the RMS error $\varepsilon^{(2)}_{r_{\boldsymbol{\zeta}^2\boldsymbol{\zeta}^2}}$ is mainly determined by the factor $\sum_{n=1}^{N} \hat{c}_n^4$. This factor can only be decreased by increasing the number of cisoids N.

5 Conclusions

In this paper, we analyzed the correlation and ergodic properties of the squared envelope of an AE SOC simulation model for mobile Rayleigh fading channels. We showed that if the Doppler frequencies of the SOC model are pair-wise different, then its squared envelope is an AE ergodic process. However, if the SOC model is parameterized in such a

[2] We pointed out in Sect. 3.5 that $\hat{\boldsymbol{\zeta}}^2(t)$ is non-AE if the IQ components of $\hat{\boldsymbol{\mu}}(t)$ are uncorrelated. Such a situation arises in the case of the GMEA and the RSM if the DPSD $S_{\boldsymbol{\mu}\boldsymbol{\mu}}(f)$ is symmetrical (scenarios: $m_\alpha = 0°, \kappa = 0$; and $m_\alpha = 90°, \kappa = 10$).

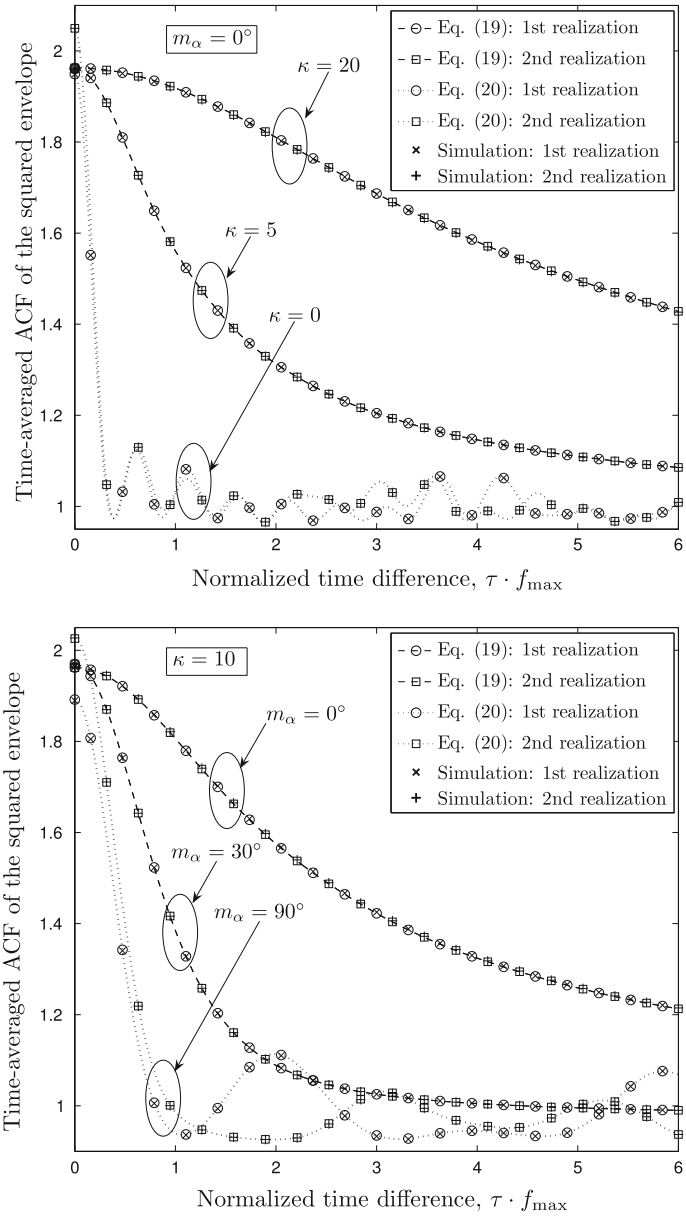

Fig. 2 Comparison between the theoretical and the empirical squared envelope ACFs of the simulation model's sample functions by considering the RSM and the von Mises PDF of the AOA ($f_{\max} = 91$ Hz, $\sigma^2_{\boldsymbol{\mu}} = 1$, and $N = 50$)

way that its IQ components are uncorrelated, then its squared envelope proves to be a non-AE process. We also evaluate the performance of the GMEA, the LPNM, and the RSM regarding their accuracy in emulating the ACF of the reference model's squared envelope. The obtained results show that the three methods provide a reasonably good

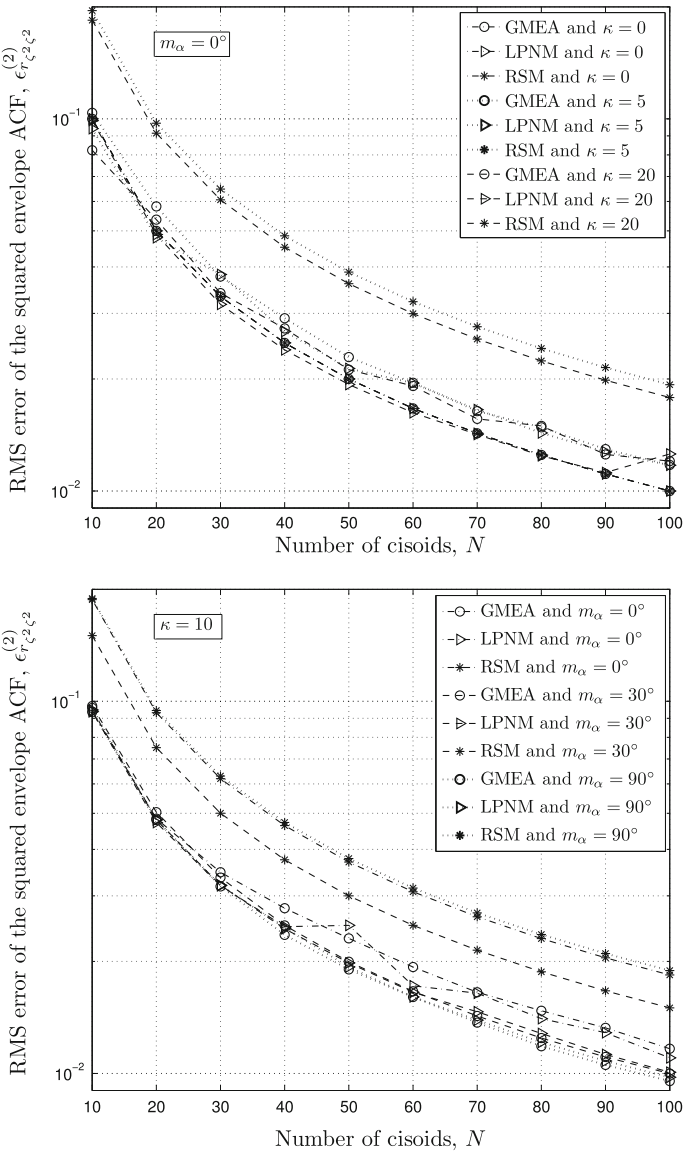

Fig. 3 RMS error $\varepsilon^{(2)}_{r_{\boldsymbol{\zeta}^2\boldsymbol{\zeta}^2}}$ of the squared envelope ACF of the simulation model designed by applying the GMEA, the LPNM, and the RSM to the von Mises PDF of the AOA ($f_{\max} = 91\,\text{Hz}$ and $\sigma^2_{\boldsymbol{\mu}} = 1$)

approximation to the channel's squared envelope ACF, although the GMEA and the LPNM perform better than the RSM. From our investigations, we can also conclude that due to the offset term inherent to the squared envelope ACF of the simulation model, the approximation to the reference model's squared envelope ACF is always worse than the approximation to the reference model's ACF and can only be improved by increasing the number of cisoids.

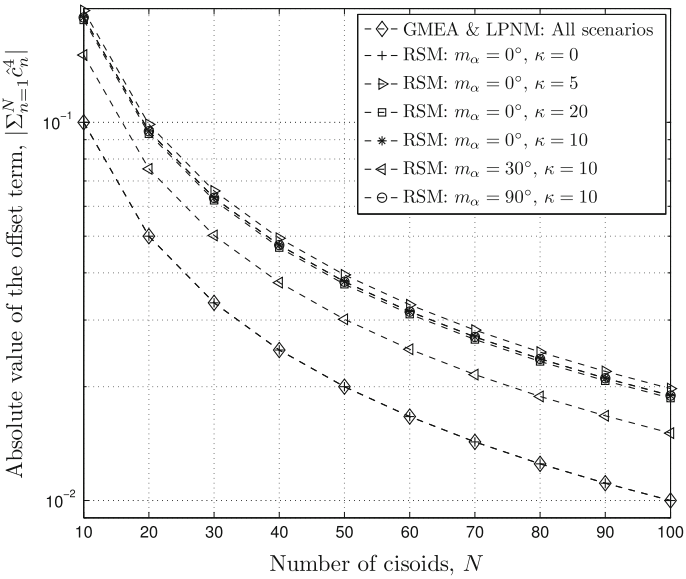

Fig. 4 Absolute value of the offset term $-\sum_{n=1}^{N} \hat{c}_n^4$ of the simulation model's squared envelope ACF as a function of N

Appendix

In this appendix, we outline the derivation of the solution presented in (20) for the TACF $r_{\hat{\zeta}^{(k)^2}\hat{\zeta}^{(k)^2}}(\tau)$ of the sample functions of $\hat{\boldsymbol{\zeta}}^2(t)$. It is assumed that the inequalities in (7) hold and Condition 1 is fulfilled. Our starting point is the expression given in (17) for $r_{\hat{\zeta}^{(k)^2}\hat{\zeta}^{(k)^2}}(\tau)$. For the case analyzed at the beginning of Sect. 3.4, the integral in (17) is different from zero in the limit $T \to \infty$ only if: $l = m = n = p$; $l = n, m = p, l \neq m$; or $l = p, m = n, l \neq n$. For the case at hand, the integral is different from zero also if $l \neq m \neq n \neq q$ and $\hat{f}_l = -\hat{f}_n$, $\hat{f}_m = -\hat{f}_p$; $\hat{f}_l = -\hat{f}_n$, $\hat{f}_p = -\hat{f}_m$; $\hat{f}_n = -\hat{f}_l$, $\hat{f}_m = -\hat{f}_p$; or $\hat{f}_n = -\hat{f}_l$, $\hat{f}_p = -\hat{f}_m$. Taking this into account, we have

$$
\begin{aligned}
r_{\hat{\zeta}^{(k)^2}\hat{\zeta}^{(k)^2}}(\tau) = \sigma_{\boldsymbol{\mu}}^4 + |r_{\hat{\mu}\hat{\mu}}(\tau)|^2 - \sum_{n=1}^{N} \hat{c}_n^4 + \sum_{l=1}^{M} \hat{c}_l^2 \exp\left\{j\left(\hat{\theta}_l + \hat{\theta}_{N-l+1}\right)\right\} \exp\left\{-j2\pi \hat{f}_l \tau\right\} \\
\times \Bigg\{ \sum_{m=1}^{M} \hat{c}_m^2 \exp\left\{-j\left(\hat{\theta}_m + \hat{\theta}_{N-m+1}\right)\right\} \exp\left\{j2\pi \hat{f}_m \tau\right\} \\
+ \sum_{n=1}^{M} \hat{c}_n^2 \exp\left\{-j\left(\hat{\theta}_n + \hat{\theta}_{N-n+1}\right)\right\} \exp\left\{-j2\pi \hat{f}_n \tau\right\} \Bigg\} \\
+ \sum_{p=1}^{M} \hat{c}_p^2 \exp\left\{j\left(\hat{\theta}_p + \hat{\theta}_{N-p+1}\right)\right\} \exp\left\{j2\pi \hat{f}_p \tau\right\} \\
\times \Bigg\{ \sum_{q=1}^{M} \hat{c}_q^2 \exp\left\{-j\left(\hat{\theta}_q + \hat{\theta}_{N-q+1}\right)\right\} \exp\left\{j2\pi \hat{f}_q \tau\right\}
\end{aligned}
$$

$$+\sum_{k=1}^{M}\hat{c}_k^2\,\exp\left\{-j\left(\hat{\theta}_k+\hat{\theta}_{N-k+1}\right)\right\}\exp\left\{-j2\pi\,\hat{f}_k\tau\right\}\Bigg\}$$

where $M = N/2$ (N is even). From the previous equation, one can verify that

$$\begin{aligned}
r_{\hat{\zeta}^{(k)^2}\hat{\zeta}^{(k)^2}}(\tau) &= \sigma_{\boldsymbol{\mu}}^4+|r_{\hat{\mu}\hat{\mu}}(\tau)|^2-\sum_{n=1}^{N}\hat{c}_n^4\\
&\quad+\sum_{l=1}^{M}\sum_{m=1}^{M}\hat{c}_l^2\,\hat{c}_m^2\,\exp\left\{j\left(\hat{\theta}_l+\hat{\theta}_{N-l+1}-\hat{\theta}_m-\hat{\theta}_{N-m+1}\right)\right\}\\
&\quad\times\Bigg\{\exp\left\{-j2\pi\left(\hat{f}_l-\hat{f}_m\right)\tau\right\}+\exp\left\{-j2\pi(\hat{f}_l+\hat{f}_m)\tau\right\}\\
&\quad+\exp\left\{j2\pi(\hat{f}_l+\hat{f}_m)\tau\right\}+\exp\left\{j2\pi(\hat{f}_l-\hat{f}_m)\tau\right\}\Bigg\}\\
&= \sigma_{\boldsymbol{\mu}}^4+|r_{\hat{\mu}\hat{\mu}}(\tau)|^2-\sum_{n=1}^{N}\hat{c}_n^4\\
&\quad+4\sum_{l=1}^{M}\sum_{\substack{m=1\\m\neq l}}^{M}\hat{c}_l^2\,\hat{c}_m^2\,\exp\left\{j(\hat{\theta}_l+\hat{\theta}_{N-l+1}-\hat{\theta}_m-\hat{\theta}_{N-m+1})\right\}\\
&\quad\times\cos\left(2\pi\hat{f}_l\tau\right)\cdot\cos\left(2\pi\,\hat{f}_m\tau\right).
\end{aligned}\tag{29}$$

Using the identity $\sum_{n=1}^{N}\sum_{m=1,m\neq n}^{N}x_n x_m^* = \left|\sum_{n=1}^{N}x_n\right|^2-\sum_{m=1}^{N}|x_m|^2$, we finally obtain (20).

References

1. Gutiérrez, C. A., & Pätzold, M. (2010). The generalized method of equal areas for the design of sum-of-cisoids simulators for mobile Rayleigh fading channels with arbitrary Doppler spectra. Wireless Communications and Mobile Computing. doi:10.1002/wcm.1154.
2. Gutiérrez, C. A., & Pätzold, M. (2010). The design of sum-of-cisoids Rayleigh fading channel simulators assuming non-isotropic scattering conditions. *IEEE Transactions on Wireless Communications, 9*(4), 1308–1314.
3. Cheng, X., Wang, C.-X., Laurenson, D. I., Salous, S., & Vasilakos, A. V. (2011). New deterministic and stochastic simulation models for non-isotropic scattering mobile-to-mobile Rayleigh fading channels. *Wireless Communication Mobile Computing, 11*(7), 829–842.
4. Zajić, A. G., & Stüber, G. L. (2008). Space-time correlated mobile-to-mobile channels: Modelling and simulation. *IEEE Transactions on Vehicular Technology, 57*(2), 715–726.
5. Pätzold, M., & Hogstad, B. O. (2004). A space-time simulator for MIMO channels based on the geometrical one-ring scattering model. *Wireless Communications and Mobile Computing, 4*, 727–737.
6. Pätzold, M., & Youssef, N. (2001). Modelling and simulation of direction-selective and frequency-selective mobile radio channels. *International Journal of Electronics and Communications, AEÜ-55*(6), 442.
7. Zhang, H., Yuan, D., Pätzold, M., Wu, Y., & Nguyen, V. D. (2010). A novel wideband space-time channel simulator based on the geometrical one-ring model with applications in MIMO-OFDM systems. *Wireless Communications and Mobile Computing, 10*(6), 758–771.
8. Rice, S. O. (1944). Mathematical analysis of random noise. *Bell System Technical Journal, 23*, 282–332.
9. Rice, S. O. (1945). Mathematical analysis of random noise. *Bell System Technical Journal, 24*, 46–156.
10. Gutiérrez, C. A. (2009). *Channel simulation models for mobile broadband communication systems.* (Doctoral dissertations at the University of Agder 16). Norway: University of Agder, Kristiansand.

11. Patel, C. S., Stüber, G. L., & Pratt, T. G. (2005). Comparative analysis of statistical models for the simulation of Rayleigh faded cellular channels. *IEEE Transactions on Communications, 53*(6), 1017–1026.
12. Li, Y., & Huang, X. (2002). The simulation of independent Rayleigh faders. *IEEE Transactions on Communications, 50*(9), 1503–1514.
13. Kotterman, W. A. T., Pedersen, G. F., & Olsen, K. (2004). Diversity properties of multiantenna small handheld terminals. *EURASIP Journal on Applied Signal Processing, 2004*(9), 1340–1353.
14. Zhao, X., Kivinen, J., Vainikainen, P., & Skog, K. (2003). Characterization of Doppler spectra for mobile communications at 5.3 GHz. *IEEE Transactions on Vehicular Technology, 52*(1), 14–23.
15. Hogstad, B. O., & Pätzold, M. (2008). On the stationarity of sum-of-cisoids-based mobile fading channel simulators. In *Proceedings of 67th IEEE Vehicular Technology Conference (VTC2008-spring)* Singapore, 2008, (pp. 400–404).
16. Pätzold, M., & Talha, B. (2007). On the statistical properties of sum-of-cisoids-based mobile radio channel simulators. In *Proceedings of 10th International Symposium on Wireless Personal Multimedia Communications (WPMC'07)*, Jaipur, India, 2007, (pp. 394–400).
17. Pätzold, M., & Gutiérrez, C. A. (2008). Level-crossing rate and average duration of fades of the envelope of a sum-of-cisoids. In *Proceedings of 67th IEEE Vehicular Technology Conference (VTC2008-spring)* Singapore, 2008, (pp. 488–494).
18. Parsons, J. D. (2000). *The mobile radio propagation channel* (2nd ed.). Chichester, UK: Wiley.
19. Jingyu, H., Xiaomin, Z., Zhijiang, X., & Limin, M. (2007). An adaptive Doppler shift estimator in mobile communication systems. *IEEE Antennas Wireless Propagation Letters, 6*, 117–121.
20. Park, G., Nam, S., Yu, T., Hong, D., & Kang, C. (2005). A modified covariance-based mobile velocity estimation method for Rician fading channels. *IEEE Communications Letters, 9*(8), 706–708.
21. Tepedelenliŏglu, C., Abdi, A., Giannakis, G. B., & Kaveh, M. (2001). Estimation of Doppler spread and signal strength in mobile communications with applications to handoff and adaptive transmission. *Wireless Communications and Mobile Computing, 1*(2), 221–242.
22. Clarke, R. H. (1968). A statistical theory of mobile radio reception. *Bell System Technical Journal, 47*, 957–1000.
23. Brigham, E. O. (1988). *The fast Fourier transform and its applications*. Englewood Cliffs, NJ: Prentice-Hall.
24. Leon-Garcia, A. (1994). *Probability and random processes for electrical engineering* (2nd ed.). New York, NY: Addison-Wesley.
25. Abdi, A., Barger, J. A., & Kaveh, M. (2002). A parametric model for the distribution of the angle of arrival and the associated correlation function and power spectrum at the mobile station. *IEEE Transactions on Vehicular Technology, 51*(3), 425–434.

Author Biographies

Carlos A. Gutiérrez received the B.E. degree in electronics and digital communication systems from the Autonomous University of Aguascalientes, Mexico, in 2002, the Advanced Studies Diploma (DEA) in signal processing and communication theory from the Polytechnic University of Catalonia, Spain, in 2005, the M.S. degree in electronics and telecommunications from CICESE, Mexico, in 2006, and the Ph.D. degree in mobile communication systems from the University of Agder, Norway, in 2009. He is an assistant professor at the electronics Department, Autonomous University of San Luis Potosi, Mexico, and a part-time lecturer and researcher at the School of Engineering, Panamericana University Campus Aguascalientes, Mexico. His research interests include modeling and simulation of mobile fading channels for broadband wireless communication systems, and physical layer aspects of OFDM and MC-CDMA systems. He has served as guest editor for the journals Modelling and Simulation in Engineering, Procedia Technology, and Research in Computing Science, as general co-chair for CIIECC 2011, as TPC co-chair for CIIECC 2012, and as TPC member for various international conferences. Dr. Gutierrez is member of the Mexican National System of Researchers (SNI), the Institute of Electrical and Electronics Engineers (IEEE), the IEEE Communications Society, and the IEEE Antennas and Propagation Society.

Matthias Pätzold received the Dipl.-Ing. and Dr.-Ing. degrees from Ruhr-University Bochum, Bochum, Germany, in 1985 and 1989, respectively, all in Electrical Engineering. In 1998, he received the habil. degree in Communications Engineering from the Technical University of Hamburg-Harburg, Hamburg, Germany. From 1990 to 1992, he was with ANT Nachrichtentechnik GmbH, Backnang, Germany, where he was engaged in digital satellite communications. From 1992 to 2001, he was with the Department of Digital Networks at the Technical University Hamburg-Harburg. In 2001, he joined the University of Agder, Grimstad, Norway, where he is a Full Professor for Mobile Communications and the Head of the Mobile Communications Group. He authored and co-authored more than 230 technical journal and conference papers. His publications received nine best paper awards. He is author of the books "Mobile Radio Channels - Modelling, Analysis, and Simulation" (in German) (Wiesbaden, Germany: Vieweg, 1999), "Mobile Fading Channels" (Chichester, U.K.: Wiley & Sons, 2002), which has been translated into Chinese in 2008, and "Mobile Radio Channels" (Chichester, U.K.: Wiley & Sons, 2011). Prof. Pätzold was the TPC Chair of ISWCS'07, the TPC Co-Chair of ATC'11, ATC'10, ICCE'10, and the Local Organizer of KiVS'01. He has been actively participating in numerous conferences serving as TPC member for more than 20 conferences within the last 3 years. He served as Keynote Speaker, Tutorial Lecturer, and Session Chair for many reputed international conferences. He is Associate Editor of the IEEE Vehicular Technology Magazine and has edited several special issues. He is a Senior Member of the IEEE. His current research interests include mobile radio communications, especially multipath fading channel modelling, multiple-input multiple-output (MIMO) systems, cooperative communication systems, vehicular-to-vehicular communications, mobile-to-mobile communications, and coded-modulation techniques for fading channels.